Coherence-based measurement of non-Markovian dynamics in an open quantum system

Yonny Yugra and Francisco De Zela
Departamento de Ciencias, Sección Física, Pontificia Universidad Católica del Perú, Apartado 1761, Lima, Peru

Álvaro Cuevas
ICFO-Institut de Ciencies Fotoniques, The Barcelona Institute of Science and Technology, 08860 Castelldefels, Barcelona, Spain

(Received 3 October 2019; revised manuscript received 26 November 2019; published 21 January 2020)

We present a theoretical scheme and its experimental proof of principle for an open quantum system undergoing Markovian and non-Markovian evolutions. We exhibit these two regimes by diagnosing them with the relative entropy of coherence of two polarization qubits playing the roles of system and ancilla. These are initially prepared in a polarization maximally entangled state of a photon pair produced by spontaneous parametric down-conversion. We induce Markovian and non-Markovian regimes in the system's dynamics with the help of two auxiliary qubits, experimentally implemented by optical paths in a layout of Sagnac and Mach-Zehnder interferometers. We replicate system-environment interactions by means of an amplitude damping channel and a suitably designed inversion of it. In our scheme, one needs only two experimentally accessible parameters to achieve Markovian and non-Markovian regimes.

DOI: 10.1103/PhysRevA.101.013822

I. INTRODUCTION

In the framework of open quantum systems, it is useful to consider the system under study and its environment as two subsystems that constitute a closed Hilbert space. In this space, the total amount of information is preserved, even though it may be exchanged between system and environment [1,2]. System-environment communications are governed by a global dynamical map that usually leads to irreversible Markovian processes where any structured information gets dissipated among the interconnected parts of the total Hilbert space. However, there are also cases in which information can flow from the environment back to the system, thereby exhibiting a non-Markovian behavior [3]. By exploiting cases like these, one could in principle engineer techniques to prevent information losses and so design robust communication protocols.

The purpose of this work is to study a suitably designed example of coherence tracking and control on an open quantum system. We identify coherence as being a quantum resource that can be generated and consumed by means of suitably designed mechanisms. This makes coherence a useful quantifier for quantum information tasks [4], while it further allows the signal of Markovian and non-Markovian evolutions [5]. In particular, the so-called *relative entropy of coherence* $C_{\rm rec}$ has been defined [4] to measure the population balance and its relative correlation according to

$$C_{\rm rec}(\rho) = S(\rho_{\rm diag}) - S(\rho). \tag{1}$$

Here, S is the von Neumann entropy [6] and $\rho_{\rm diag}$ denotes the matrix obtained by deleting all off-diagonal elements in the density matrix ρ.

When a system s undergoes a Markovian process, its state ρ_s evolves in time according to $\rho_s(t) = \Lambda_s(t)\rho_s(0)$, with $\Lambda_s(t)$ being a completely positive and divisible map. Such a map cannot increase the amount of coherence [4,7]. Hence, one may assume that the monotonic derivative condition $\dot{C}_{\rm rec}[\rho_s(t)]\leqslant 0$ signals a non-Markovian dynamics on the system space. However, it has been shown that this condition fails to diagnose Markovianity in some cases, in particular when the amplitude damping channel is involved [5]. This channel represents an important dissipation mechanism that can lead, for instance, to bit-flip errors. These errors do not occur when dissipation comes only from phase damping, a channel that has been much studied lately [8–15]. It is thus worth addressing the amplitude damping channel in order to get additional insight about information losses and recovery. Fortunately, there is a way around the inappropriateness of the derivative condition $\dot{C}_{\rm rec}[\rho_s(t)]\leqslant 0$. Indeed, one may resort to a modified rule for Markovianity that reads $\dot{C}_{\rm rec}[\rho_{a,s}(t)]\leqslant 0$, where the compound state $\rho_{a,s}$ describes the system of interest (s) together with some ancilla (a). Accordingly, for the state evolution $\rho_{a,s}(t) = \mathcal{E}[\rho_{a,s}(0)]$, with a bipartite process $\mathcal{E} = \mathbb{I}_a \otimes \Lambda_s$, the violation of the last extended monotonicity implies the appearance of non-Markovianity [5,16–18].

In this work, we analyze the evolution of $C_{\rm rec}$ for a state $\rho_{a,s}$ in which system and ancilla are encoded in two polarization photon qubits. System s interacts with two additional degrees of freedom that represent two environment qubit spaces (e and d). One of them has been implemented by the two output modes of a Sagnac interferometer, while the other qubit corresponds to two possible detection times due to an unbalanced nested structure within a Mach-Zehnder interferometer (MZI). With this scheme, we are able to generate different regimes of Markovian and non-Markovian dynamics by tuning only two experimental parameters. Such regimes and their experimental realizations constitute the first steps towards the implementation of related protocols for

efficient information tracking and recovery of information losses.

Our study complements previous research related to phase-damping channels, where the open system was either a single polarized photon or a pair of polarized photons [8–15]. In most of those cases, the environment was given by the photon's frequency mode, ruled by some frequency distribution whose evolution depended on the polarization state, thereby giving rise to non-Markovian processes. In other cases, the role played by the photon's frequency distribution was played by the photon's spatial distribution, i.e., the distribution of the photon's emission angles [12]. The degree of non-Markovianity was assessed through the rate of change σ of the trace distance $D(\rho_1, \rho_2) = \mathrm{Tr}\,|\rho_1 - \rho_2|/2$ between states $\rho_1(t)$ and $\rho_2(t)$, i.e., through $\sigma[t, \rho_1(0), \rho_2(0)] = \dot{D}[\rho_1(t), \rho_2(t)]$. In terms of σ, one defines the measure $\mathcal{N} = \max_0 \int_{\sigma>0} \sigma[t, \rho_1(0), \rho_2(0)]dt$, where $\max_0$ means the maximum over all possible pairs of initial states $\rho_1(0)$ and $\rho_2(0)$. What $\mathcal{N}$ measures is thus the total increase of the trace distance during the system's evolution, and this is usually interpreted as a quantifier of the maximal amount of information that comes from the environment back to the system. This interpretation is based on the assumption that similarity between quantum states is a property from which one can draw conclusions about quantum resources. However, care should be exercised when making such an assumption [19,20]. Indeed, two states may be very close to each other in terms of the trace distance as well as in terms of, say, the Bures distance $D_B(\rho_1, \rho_2) = \sqrt{2(1 - \sqrt{F(\rho_1, \rho_2)})}$, where $F(\rho_1, \rho_2) = (\mathrm{Tr}\sqrt{\sqrt{\rho_1}\rho_2\sqrt{\rho_1}})^2$ is Uhlmann's fidelity [21]. In spite of being close to each other, two states can nonetheless have very different physical properties, e.g., one being separable and the other entangled [22]. In order to assess, for instance, information recovery when employing quantum resources, it is advisable to study different features such as distinguishability between quantum states as well as the amount of coherence. Appropriate quantifiers should then be introduced in each case.

Our goal is to employ coherence as a tool to diagnose information recovery in terms of the total increase of the relative entropy of coherence. To this end, we must implement some accompanying non-Markovian evolution and see how much control we can have over it. Here we present a viable approach and its experimental proof of principle by addressing the amplitude damping channel. Our all-optical approach requires polarization and path qubits alone. This suggests a possible complementary role that such an approach could have when dealing with phase damping and with various degrees of freedom that might enter more sophisticated scenarios. The results we report below should serve to increase our understanding of non-Markovian processes and the degree of control we might have upon them.

II. THEORETICAL MODEL

A. Non-Markovianity measure

Similarly to the measure $\mathcal{N}$, which involves trace distance, there is a measure that involves the relative entropy of coherence. As we said before, for the purposes of addressing the amplitude damping channel, this measure should be applied to the bipartite system that comprises the system under study and some ancilla. This bipartite system should evolve according to $\rho_{a,s}(t) = \mathcal{E}[\rho_{a,s}(0)]$, with $\mathcal{E} = \mathbb{I}_a \otimes \Lambda_s$. The required measure is then given by [5]

$$\mathcal{N}_{\mathrm{rec}}^{(S)} = \max_{\rho_{a,s}(0)} \int_{\dot{C}_{\mathrm{rec}}(\rho_{a,s}(t))>0} \dot{C}_{\mathrm{rec}}[\rho_{a,s}(t)]dt. \tag{2}$$

We see that $\mathcal{N}_{\mathrm{rec}}^{(S)}$ evaluates the monotonicity $C_{\mathrm{rec}}[\mathcal{E}(\rho_{a,s})] \leqslant C_{\mathrm{rec}}(\rho_{a,s})$. As it occurs with $\mathcal{N}$, measure $\mathcal{N}_{\mathrm{rec}}^{(S)}$ also prescribes that we should seek for the maximum over all possible initial states $\rho_{a,s}(0)$, which implies an optimization procedure that is generally a hard task. Fortunately, in our case we can replace $\mathcal{N}_{\mathrm{rec}}^{(S)}$ by a simpler quantifier that is based on the maximally entangled system-ancilla state $\rho_{a,s}(0) = \frac{1}{2}(|00\rangle + |11\rangle)(\langle 00| + \langle 11|)$. With reference to this initial state, we can introduce and use henceforth the following expression for a non-Markovian quantifier [5]:

$$\mathcal{N}_{\mathrm{rec}} \equiv \int_{\dot{C}_{\mathrm{rec}}(\rho_{a,s}(t))>0} \dot{C}_{\mathrm{rec}}[\rho_{a,s}(t)]dt. \tag{3}$$

B. Dynamical process

Our proposed evolution contains two steps. The first step models the usual amplitude damping (AD) channel [6], whose action describes the excitation of e by the relaxation of s. This mechanism can be simulated by the transitions $|V\rangle_s|0\rangle_e \to |V\rangle_s|0\rangle_e$ and $|H\rangle_s|0\rangle_e \to \sqrt{1-\eta_1}\,|H\rangle_s|0\rangle_e + \sqrt{\eta_1}\,|V\rangle_s|1\rangle_e$, where η_1 is the damping parameter, $|H\rangle_s$ ($|V\rangle_s$) is the horizontal (vertical) polarization of a photon, while $|0\rangle_e$ and $|1\rangle_e$ stand for the two spatial modes of a Sagnac interferometric configuration. We have taken $|V\rangle_s$ and $|0\rangle_e$ as "ground" states and $|H\rangle_s$ and $|1\rangle_e$ as "excited" states. The associated transformation that couples system (polarization) with environment (spatial modes) from t_0 to t_1 is described by a unitary operator $U_{(s,e)}(t_1, t_0)$, whose internal structure and optical implementation will be discussed later. The second step, which takes place between t_1 and t_2, has been suitably designed to effectively generate an antiamplitude damping (A-AD) channel that reverses the previous decoherence effect. Its mechanism involves, besides the s and e spaces, also the photon arrival time, which is implemented by resorting to an additional qubit, the d qubit ($|0\rangle_d$ and $|1\rangle_d$). The associated evolution operator $U_{(s,e,d)}(t_2, t_1)$ depends therefore on three qubits, the explicit formulation of which is given below.

If we consider an uncoupled, normalized initial state $|\psi(t_0)\rangle_{(s,e)} = (\alpha|H\rangle_s + \beta|V\rangle_s)|0\rangle_e$, the first step of the evolution reads

$$\begin{aligned} |\psi(t_1)\rangle_{(s,e)} &= U_{(s,e)}(t_1, t_0)\,|\psi(t_0)\rangle_{s,e} \\ &= (\alpha\sqrt{1-\eta_1}\,|H\rangle_s + \beta\,|V\rangle_s)\,|0\rangle_e \\ &\quad + \alpha\sqrt{\eta_1}\,|V\rangle_s\,|1\rangle_e\,. \end{aligned} \tag{4}$$

For the second step we seek to implement an AD channel in which the damping parameter is changed from η to something proportional to $1 - \eta$. Because of this an increase in η translates into a population *increase* of the "excited" state $|H\rangle_e$, i.e., something contrary to what happens with the usual AD channel, which depopulates the excited state. It is in this

way that we turn the AD channel into an A-AD channel. Our sought-after process can be realized, for instance, by the following transformation:

$$|\psi(t_2)\rangle_{s,e} = [\alpha\sqrt{1-\eta_1(1-\eta_2)}\,|H\rangle_s + \beta\,|V\rangle_s]\,|0\rangle_e + \alpha\sqrt{\eta_1(1-\eta_2)}\,|V\rangle_s\,|1\rangle_e\,. \tag{5}$$

Here, η_2 is the running antidamping parameter, while η_1 remains fixed during this step. Thus, the role played by η_1 in (4) is played by $1-\eta_2$ in (5).

Since the first step is equivalent to a completely positive (CP) map Λ acting on s alone, it admits the following representation:

$$\rho_s(t_1) = \Lambda[\rho_s(t_0)] = \sum_{i=0}^{1} K_i \rho_s(t_0) K_i^\dagger, \tag{6}$$

where $K_i \equiv \langle i|_e U_{s,e}(t_1,t_0)|0\rangle_e$ are the associated Kraus operators [6]. Thus, such a process describes a Markovian evolution in its more formal definition [2,23]. On the other hand, in the second step we have a non-CP map for $\eta_1 \neq 0$ and $\eta_2 \neq 0$, which corresponds to a non-Markovian dynamics [24,25]. With our choice of $|V\rangle$ as "ground" state, the Kraus operators for the AD channel of the first step read

$$K_0 = \begin{pmatrix} \sqrt{1-\eta_1} & 0 \\ 0 & 1 \end{pmatrix}, \qquad K_1 = \begin{pmatrix} 0 & 0 \\ \sqrt{\eta_1} & 0 \end{pmatrix}. \tag{7}$$

Since the second step we propose is intrinsically non-Markovian, we stress that there is no Kraus decomposition associated to Eq. (5) from t_1 to t_2 but only from t_0 to t_2 according to

$$K_0 = \begin{pmatrix} \sqrt{1-\eta_1(1-\eta_2)} & 0 \\ 0 & 1 \end{pmatrix}, \quad K_1 = \begin{pmatrix} 0 & 0 \\ \sqrt{\eta_1(1-\eta_2)} & 0 \end{pmatrix}. \tag{8}$$

One can easily check that for an initial maximally entangled state $\rho_{a,s}(t_0) = \frac{1}{2}(|00\rangle + |11\rangle)(\langle 00| + \langle 11|)$, where the system is in a completely mixed state $\rho_s(t_0) = \mathrm{Tr}[\rho_{a,s}(t_0)] = \frac{1}{2}\mathbb{I}_s$, the two-step evolution from t_0 to t_2 simply leads to

$$\rho_s(t_2) = \frac{1}{2}\begin{pmatrix} 1-\eta_1(1-\eta_2) & 0 \\ 0 & 1+\eta_1(1-\eta_2) \end{pmatrix}. \tag{9}$$

In our proposal, when the AD channel reaches its maximum level ($\eta_1 = 1$) at the end of the first step, the population of the excited state $|H\rangle_s$ is totally depleted and the system is in its ground state $\rho_s(t_1) = |V\rangle_s\langle V|$. After completion of the second step, when $\eta_2 = 1$, the system is in state $\rho_s(t_2) = \frac{1}{2}\mathbb{I}_s = \rho_s(t_0)$. As we shall see, in cases like this the relative entropy of coherence (C_{rec}) goes from $C_{\mathrm{rec}} = 1$ at t_0 to $C_{\mathrm{rec}} = 0$ at t_1, and then back to $C_{\mathrm{rec}} = 1$ at t_2. Other processes are also possible, in which partial loss and recovery of coherence may occur at a given rate.

C. Non-Markovian quantifier

As already stated, we start with qubits a and s in the maximally entangled state $\rho_{a,s}(t_0) = |\psi(t_0)\rangle_{a,s}\langle\psi(t_0)|$, where the ancilla and system are polarization qubits: $|\psi(t_0)\rangle_{a,s} = \frac{1}{\sqrt{2}}(|H\rangle_a\,|H\rangle_s + |V\rangle_a\,|V\rangle_s)$. The e qubit starts in its ground state $|0\rangle_e$, which corresponds to a propagation path. The first step in the evolution of the a-s state is defined by

$$\rho_{(a,s)}(t_1) = \mathrm{Tr}_e[\mathcal{E}_1[\rho_{(a,s)}(t_0)\otimes|0\rangle_e\langle 0|]\mathcal{E}_1^\dagger] = \mathrm{Tr}_e[\rho_{(a,s,e)}(t_1)], \tag{10}$$

where $\mathcal{E}_1 = \mathbb{I}_a \otimes U_{(s,e)}(t_1,t_0)$.

The second step in the evolution of the a-s state is defined by

$$\rho_{(a,s)}(t_2) = \mathrm{Tr}_e[\mathrm{Tr}_d(\mathcal{E}_2[\rho_{(a,s,e)}(t_1)\otimes|0\rangle_d\langle 0|]\mathcal{E}_2^\dagger)] = \mathrm{Tr}_e[\rho_{(a,s,e)}(t_2)], \tag{11}$$

where $\mathcal{E}_2 = \mathbb{I}_a \otimes U_{(s,e,d)}(t_2,t_1)$ is the corresponding full operator. In this case, we have to trace out both environment spaces, e and d, in order to extract the information stored in the a-s system. Since the above dynamics leads to $\dot{C}_{\mathrm{rec}}[\rho_{a,s}(t)] > 0$ for $t_1 \leqslant t \leqslant t_2$, the non-Markovian quantifier of Eq. (3) is given by

$$\mathcal{N}_{\mathrm{rec}} = C_{\mathrm{rec}}[\rho_{a,s}(t_2)] - C_{\mathrm{rec}}[\rho_{(a,s)}(t_1)]. \tag{12}$$

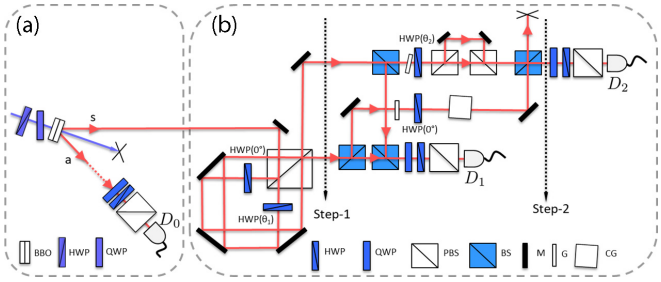

FIG. 1. Diagram of the experiment. (a) SPDC source and a-photon tomography. (b) Implementation of the two-step channel: a SI-based AD channel (first step) and a MZI-based A-AD channel (second step). After the angular rotation $\theta_1(\eta_1)$ made by U_{HWP}, the undamped (damped) light exits the SI through its bottom (top) output mode $|0\rangle_e$ ($|1\rangle_e$). The angular rotation $\theta_2(\eta_2)$ made by U'_{HWP} sends the damped light back to $|0\rangle_e$. A tilting glass G provides the relative phase $\delta_e = \pm\pi/2$, which is required for interference at the last beam splitter. Another G and a thick compensation glass (CG) are used to compensate relative time delays between $|0\rangle_e$ and $|H\rangle_s$ after $\theta_2(\eta_2)$, while $|V\rangle_s$ is filtered out from ancilla-system coincidences in the nested MZI.

D. All-optical implementation

In what follows, we describe how the required unitary transformations that correspond to the Markovian and non-Markovian evolutions can be implemented using all-optical setups. Figure 1 shows a scheme of the complete arrangement.

1. First step: Markovian evolution

As we said before, we can implement the AD channel by means of a Sagnac interferometer (SI) [see Fig. 1, lower-left corner of panel (b)]. The associated unitaries read

$$U_{\mathrm{SI}}^{(s,e)}(\theta_1) = U_{\mathrm{PBS}}\big(U_{\mathrm{HWP0}}^{(s,e)}(\theta_1)\big)U_{\mathrm{PBS}},$$
$$U_{\mathrm{HWP0}}^{(s,e)}(\theta_1) = H_s(0)\otimes|1\rangle_e\langle 1| + H_s(\theta_1)\otimes|0\rangle_e\langle 0|,$$
$$U_{\mathrm{PBS}} = |H\rangle_s\langle H|\otimes\mathbb{I}_e + |V\rangle_s\langle V|\otimes\sigma_e^x, \tag{13}$$

where $U_{\mathrm{HWP0}}^{(s,e)}$ corresponds to the action of the half-wave plates (HWPs) on each path of the SI, and U_{PBS} corresponds to the action of the polarizing beam splitter. Here, σ_e^x is Pauli's x matrix acting on the path qubit. $H_s(\theta)$ is the unitary that represents the action of the half-wave plate on the system (polarization) qubit: $H_s(\theta) = \cos(2\theta)\sigma_s^z + \sin(2\theta)\sigma_s^x$.

The total unitary that acts on the three qubits—ancilla, system, and e path—is given by

$$U_{\mathrm{SI}}^{(a,s,e)}(\theta_1) = \mathbb{I}_a \otimes U_{\mathrm{SI}}^{(s,e)}(\theta_1). \tag{14}$$

Unitary $U_{\mathrm{SI}}^{(a,s,e)}(\theta_1)$ acts on the input state $\rho_{(a,s,e)}(t_0) = \rho_{(a,s)}(t_0) \otimes |0\rangle_e \langle 0|$, with $\rho_{(a,s)}(t_0) = \frac{1}{2}(|HH\rangle + |VV\rangle)(\langle HH| + \langle VV|)$. For $t_0 \leqslant t \leqslant t_1$, we then have

$$\begin{aligned}\rho_{(a,s)}(\theta_1) &= \mathrm{Tr}_e\left[U_{\mathrm{SI}}^{(a,s,e)}(\theta_1)\rho_{(a,s,e)}(t_0)\left[U_{\mathrm{SI}}^{(a,s,e)}(\theta_1)\right]^\dagger\right] \\ &= \frac{1}{2}\begin{pmatrix} \cos^2(2\theta_1) & 0 & 0 & -\cos(2\theta_1) \\ 0 & \sin^2(2\theta_1) & 0 & 0 \\ 0 & 0 & 0 & 0 \\ -\cos(2\theta_1) & 0 & 0 & 1 \end{pmatrix}.\end{aligned} \tag{15}$$

From the eigenvalues of $\rho_{(a,s)}$ and its associated diagonal matrix $\rho_{(a,s)}^{\mathrm{diag}}$ we obtain, as per Eq. (1),

$$\begin{aligned}C_{\mathrm{rec}}(\theta_1) = \frac{1}{\log 16}\Bigg\{ &\ln 4 - 2\cos^2(2\theta_1)\ln\left[\frac{\cos^2(2\theta_1)}{2}\right] \\ &+ [3 + \cos(4\theta_1)]\ln\left[\frac{3+\cos(4\theta_1)}{4}\right]\Bigg\}.\end{aligned} \tag{16}$$

The values taken by $C_{\mathrm{rec}}(\theta_1)$ in the range $0 \leqslant \theta_1 \leqslant \pi/4$ correspond to a Markovian process ($\mathcal{N}_{\mathrm{rec}} = 0$), according to the quantifier given by Eq. (3).

Written in terms of $\eta_1 = \sin^2(2\theta_1)$, the density operator $\rho_{(a,s)}$ reads

$$\rho_{(a,s)}(\eta_1) = \frac{1}{2}\begin{pmatrix} 1-\eta_1 & 0 & 0 & \sqrt{1-\eta_1} \\ 0 & \eta_1 & 0 & 0 \\ 0 & 0 & 0 & 0 \\ \sqrt{1-\eta_1} & 0 & 0 & 1 \end{pmatrix}. \tag{17}$$

As for the density matrix of the system, $\rho_s = \mathrm{Tr}_a(\rho_{(a,s)})$, it is given by

$$\rho_s(\eta_1) = \frac{1}{2}\begin{pmatrix} 1-\eta_1 & 0 \\ 0 & 1+\eta_1 \end{pmatrix}. \tag{18}$$

This ρ_s corresponds, as it should, to the evolution of $\rho_s(0) = \frac{1}{2}\mathbb{I}_s$ under the AD channel.

2. *Second step: Non-Markovian evolution*

In the second step we perform two-qubit, ancilla-system tomography of state $\rho_{a,s}(\theta_2)$ by coincidence measurements in detectors D_0 and D_2. Photon beams leading to detector D_1 are blocked. What remains after the SI is therefore a Mach-Zehnder–type setup [see Fig. 1, middle part of panel (b)]. As we said before, the upper branch of this interferometric arrangement has a HWP oriented to θ_2, followed by an additional structure that consists of two polarizing beam splitters (PBSs) and two mirrors. They serve the purpose of increasing the optical path for vertically polarized photons by more than the photon's coherence length, which in our case was experimentally estimated to be 10 μm. The above mechanism is equivalent to enlarging the Hilbert space by including the photon detection time (d qubit) as an additional environment space. Unlike the vertical polarization in the upper branch, the horizontal one and any polarization in the lower branch are temporally balanced by the help of a HWP oriented to 0°, together with compensation glasses for additional adjustments of the path lengths. Hence, only the horizontal polarization in the upper branch can contribute to the coherent coincidences together with the ancillary photons. It is by this polarization-dependent coincidence detection that we implement the A-AD channel.

The unitary action of the Mach-Zehnder (MZ)–type setup is given by $U_{\mathrm{MZ}}^{(s,e,d)}(\theta_2) = U_{\mathrm{BS}}^{(e)} U_{\mathrm{HWPc}}^{(s,e,d)}(\theta_2)$, where

$$U_{\mathrm{BS}}^{(e)} = \mathbb{I}_s \otimes \frac{1}{\sqrt{2}}\left(\sigma_e^x + \sigma_e^z\right) \otimes \mathbb{I}_d \tag{19}$$

corresponds to the action of the beamsplitter on the e qubit, leaving the s and d qubits unchanged, while

$$U_{\mathrm{HWPc}}^{(s,e,d)}(\theta_2) = U_c^{(s,e,d)} U_{\mathrm{HWP}}^{(s,e)}(\theta_2) \tag{20}$$

is a unitary operator that acts on the three qubits: the system qubit (s), the path environment qubit (e), and the detection qubit (d).

The unitary $U_{\mathrm{HWPc}}^{(s,e,d)}$ in Eq. (20) is a product of two unitaries:

$$\begin{aligned}U_{\mathrm{HWP}}^{(s,e)}(\theta_2) &= [H_s(0) \otimes |0\rangle_e\langle 0| + e^{i\delta} H_s(\theta_2) \otimes |1\rangle_e\langle 1|] \otimes \mathbb{I}_d \\ U_c^{(s,e,d)} &= |V\rangle_s\langle V| \otimes |1\rangle_e\langle 1| \otimes \sigma_d^x \\ &\quad + |H\rangle_s\langle H| \otimes |1\rangle_e\langle 1| \otimes \mathbb{I}_d + \mathbb{I}_s \otimes |0\rangle_e\langle 0| \otimes \mathbb{I}_d.\end{aligned} \tag{21}$$

$U_{\mathrm{HWP}}^{(s,e)}(\theta_2)$ acts on the s and e qubits, leaving d unchanged. Depending on the path, $|0\rangle_e$ or $|1\rangle_e$, the s qubit is submitted to a polarization transformation by the HWP's unitary $H_s(\theta_2)$, or else it is left unchanged by $H_s(0)$, whose corresponding HWP is set on the branch belonging to qubit $|0\rangle_e$ to compensate the optical-path increment associated to the other HWP. The second action of $U_{\mathrm{HWPc}}^{(s,e,d)}(\theta_2)$ is made by $U_c^{(s,e,d)}$, which belongs to the additional setup on the upper branch of the MZI. Here, vertically polarized photons $|V\rangle_s$ traveling along path $|1\rangle_e$ are submitted to a change from path $|0\rangle_d$ to $|1\rangle_d$ by σ_d^x. Horizontally polarized photons $|H\rangle_s$ traveling along path $|1\rangle_e$ are left unchanged, as is also the case with photons traveling along path $|0\rangle_e$, the lower branch of the MZI.

In order to include the ancilla, we extend $U_{\mathrm{MZ}}^{(s,e,d)}(\theta_2)$ to $U_{\mathrm{MZ}}^{(a,s,e,d)}(\theta_2) = \mathbb{I}_a \otimes U_{\mathrm{MZ}}^{(s,e,d)}(\theta_2)$. Finally, the unitary transformation that is performed by the whole setup reads

$$U_T^{(a,s,e,d)}(\theta_1,\theta_2) = U_{\mathrm{MZ}}^{(a,s,e,d)}(\theta_2)\left(U_{\mathrm{SI}}^{(a,s,e)}(\theta_1) \otimes \mathbb{I}_d\right), \tag{22}$$

where $U_{\mathrm{SI}}^{(a,s,e)}(\theta_1)$ has been defined in Eq. (14).

The input state of the total system is

$$\begin{aligned}\rho_{(a,s,e,d)}^{(\mathrm{in})}(0) &= |\psi\rangle_{(a,s)}\langle\psi| \otimes |0\rangle_e\langle 0| \otimes |0\rangle_d\langle 0|, \\ |\psi\rangle_{(a,s)} &= \frac{1}{\sqrt{2}}(|H\rangle_a |H\rangle_s + |V\rangle_a |V\rangle_s).\end{aligned} \tag{23}$$

The output state is then given by

$$\rho^{(\mathrm{out})}_{(a,s,e,d)}(\theta_1,\theta_2) = U_T^{(a,s,e,d)}\rho^{(\mathrm{in})}_{(a,s,e,d)}(0)\big(U_T^{(a,s,e,d)}\big)^{\dagger}. \quad (24)$$

By tracing out the d qubit from the above output state, we obtain $\rho^{(\mathrm{out})}_{(a,s,e)} = \mathrm{Tr}_d\,(\rho^{(\mathrm{out})}_{(a,s,e,d)})$. This state is submitted to a coincidence measurement at detectors D_0 and D_2. Qubit $|1\rangle_e$ corresponds to the path leading to D_2. Accordingly, we obtain the reduced, un-normalized ancilla-system state by projecting on $|1\rangle_e$ and tracing out the e qubit: $\tilde{\rho}^{(\mathrm{out})}_{(a,s)} = \mathrm{Tr}_e\,(\rho^{(\mathrm{out})}_{(a,s,e)}\,|1\rangle_e\langle 1|)$. The normalized ancilla-system state that describes our measurement results is thus given by

$$\rho^{(\mathrm{out})}_{(a,s)} = \frac{\tilde{\rho}^{(\mathrm{out})}_{(a,s)}}{\mathrm{Tr}_{a,s}\left(\tilde{\rho}^{(\mathrm{out})}_{(a,s)}\right)}. \quad (25)$$

This is the sate we use to calculate $C_{\mathrm{rec}}(\rho_{(a,s)})$ and $\mathcal{N}_{\mathrm{rec}}$ [see Eqs. (1) and (3)]. Written in terms of the damping parameters $\eta_{i=1,2}$, the ancilla-system output density matrix reads

$$\rho^{(\mathrm{out})}_{(a,s)} = \frac{1}{2-2\cos(\delta)\sqrt{(1-\eta_1)\eta_1\eta_2}}\begin{pmatrix} 1-2\cos(\delta)\sqrt{(1-\eta_1)\eta_1\eta_2}-\eta_1(1-\eta_2) & 0 & 0 & \sqrt{1-\eta_1}-e^{i\delta}\sqrt{\eta_1\eta_2} \\ 0 & \eta_1(1-\eta_2) & 0 & 0 \\ 0 & 0 & 0 & 0 \\ \sqrt{1-\eta_1}-e^{-i\delta}\sqrt{\eta_1\eta_2} & 0 & 0 & 1 \end{pmatrix}. \quad (26)$$

Setting $\delta = \pi/2$ and tracing over the ancilla, we get the system state $\rho^{(\mathrm{out})}_s = \mathrm{Tr}_a\,(\rho^{(\mathrm{out})}_{(a,s)})$ that was previously announced in Eq. (9):

$$\rho^{(\mathrm{out})}_s = \frac{1}{2}\begin{pmatrix} 1-\eta_1(1-\eta_2) & 0 \\ 0 & 1+\eta_1(1-\eta_2) \end{pmatrix}. \quad (27)$$

This is our sought-after result. The output system state corresponds to having evolved $\rho_s(0) = \frac{1}{2}\mathbb{I}_s$ by an A-AD channel. Indeed, $\rho^{(\mathrm{out})}_s$ above can be obtained from state ρ_s of Eq. (18) through the replacement of η_1 by $\eta_1(1-\eta_2)$. Keeping η_1 fixed while letting η_2 go from zero to 1, we get an A-AD evolution.

In Fig. 2 we show the theoretically calculated $C_{\mathrm{rec}}(\rho^{(\mathrm{out})}_{(a,s)})$ for values of $\eta_{1,2}$ in the range [0,1], i.e., for $\theta_{1,2}$ in the range $[0,\pi/4]$, and $\delta = \pi/2$ [see Eq. (26)]. For fixed values of θ_2 we see a coherence decrease that depends on θ_1, while for any fixed $\theta_1 \neq 0$ we see a coherence revival when θ_2 grows up. This full control of coherence allows us to recover the initial bipartite state and its associated polarization coherence during the evolution. We should stress that any of the two output ports of the final beamsplitter can be used for this purpose.

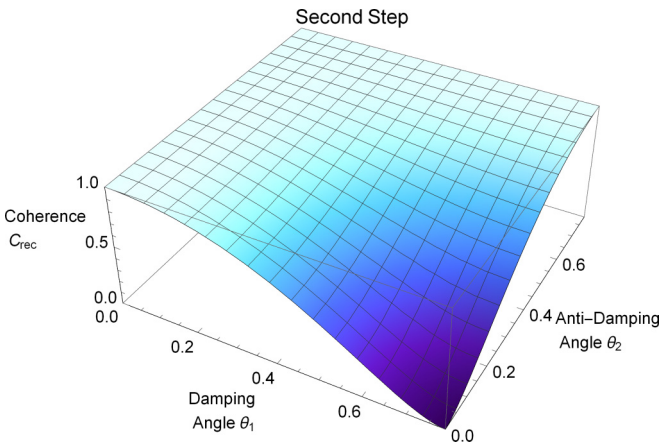

FIG. 2. Theoretically calculated $C_{\mathrm{rec}}[\rho_{a,s}(t_2)]$ for both the damping angle θ_1 and the antidamping angle θ_2 varying in the range $[0,\pi/4]$.

III. EXPERIMENTAL SETUP AND RESULTS

In our setup, polarization-entangled photon pairs are created by spontaneous parametric down-conversion (SPDC) in two barium-beta-borate (BBO) crystals having their optical axes oriented perpendicular to one another and being pumped with a cw laser diode (400 nm, 0.7 nm linewidth, 37.5 mW), as shown in Fig. 1(a). The entangled s and a photons have a wavelength of 800 nm. The a photon is directly sent to a tomography stage composed by a quarter-wave plate (QWP), a half-wave plate, and a consecutive polarizing beam splitter, while the s photon is injected into the bulk-optics setup before entering another complementary tomography stage [26]. Photons are collected with multimode fiber optics and registered within a coincidence window of 10.42 ns by synchronized avalanche photodetectors (APDs).

The input state $\rho^{(\mathrm{in})}_{(a,s)} = |\psi\rangle_{(a,s)}\langle\psi|$ was produced with the required purity, as can be seen in Fig. 3, which shows the result of a tomographic characterization. The purity of $\rho^{(\mathrm{in})}_{(a,s)}$ was better than 92% in each experimental run. To achieve this purity, we set a HWP and a tilted QWP before the BBO crystals so as to produce states of the form $|\psi\rangle_{(a,s)} = \cos\theta|H\rangle|H\rangle + \exp(i\phi)\cos\theta|V\rangle|V\rangle$. By rotating and tilting the QWP, we could achieve the required purity of $\rho^{(\mathrm{in})}_{(a,s)}$, as tested by standard two-qubit tomography assisted by maximum-likelihood estimation [26]. This method proved to perform better than an alternative one in which we employed a calcite crystal and a Glan-Thompson prism.

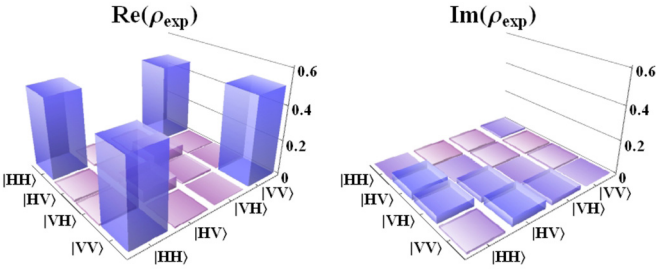

FIG. 3. Measured density matrix of the initial state $\rho^{(\mathrm{in})}_{(a,s)}$. The targeted state is a pure, maximally entangled one: $|\psi\rangle_{(a,s)}\langle\psi|$. Measured purity is better than 92%.

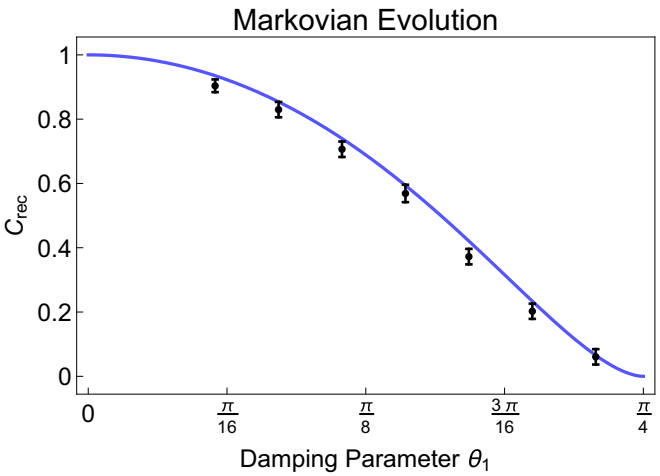

FIG. 4. Experimental results of $C_{\rm rec}(\rho_{a,s})$ at the first step of the evolution. We exhibited coherence loss by varying θ_1 so as to scan $C_{\rm rec}(\rho_{a,s})$ over a wide range of values between 1 and zero. Error bars come from the standard deviation over ten measurements.

As for the first step of the evolution, we implemented it by means of a displaced SI [see Fig. 1(b)]. The s photon of the initial, bipartite state $|\psi(t_0)\rangle_{a,s} = \frac{1}{\sqrt{2}}(|H\rangle_a |H\rangle_s + |V\rangle_a |V\rangle_s)$ propagates along the upper input mode, which represents the environment ground state $|0\rangle_e$, whence the $|H\rangle$ ($|V\rangle$) component of the s photon circulates in the clockwise (counterclockwise) trajectory inside the SI. Following [27], we implemented the AD channel by an angular rotation $\theta_1(\eta_1) = \frac{1}{2}\arccos(-\sqrt{1-\eta_1})$ of the half-wave plate that intersects the clockwise trajectory. Another HWP, set to $\theta_0 = 0$, is placed in the counterclockwise trajectory to compensate the relative time delay. This HWP introduces only a relative phase shift of π between H and V polarization states. Undamped light exits the SI—after having followed the counter-clockwise path—through the horizontal (lower) output mode of the SI's PBS. This mode corresponds to $|0\rangle_e$, while the complementary, vertical (upper) output mode is associated to $|1\rangle_e$. Thereafter, we perform the first-step's two-qubit tomography of qubits s and a [26]. This involves coincidence measurements at detectors D_0 and D_1 (see Fig. 1). Figure 4 shows our measurements of $C_{\rm rec}$ for the first step, during which the Markovian evolution takes place. It corresponds to coincidence measurements at detectors D_0 and D_1. Only the Sagnac part of the arrangement was involved. Here, $C_{\rm rec}$ goes from one (for $\theta_1 = 0$) to zero (for $\theta_1 = \pi/4$). The three beam splitters that follow the SI—two at the lower branch and one at the upper branch—have the sole purpose of allowing us to perform coincidence measurements at detectors D_0 and D_1 first and at D_0 and D_2 afterwards, without mounting and demounting the required setups. In this way, having fixed all optical components, we just block the unrequired photon beams.

The setup that implements the second step of the process is essentially a MZI with time delay for one polarization. The lower branch has a HWP set to 0°, while at the upper branch there is a second HWP set at $\theta_2 = \frac{1}{2}\arccos(-\sqrt{1-\eta_2})$, allowing tuning of the damping factor η_2 of the A-AD channel. The upper branch of the MZI subdivides into two orthogonally polarized modes of a nested structure. Its vertically

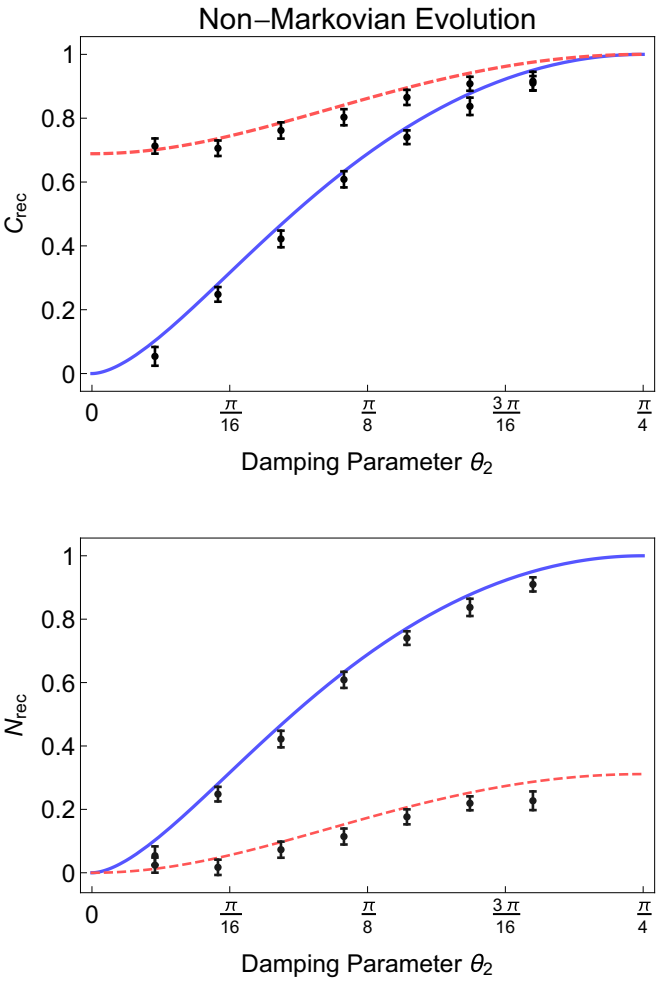

FIG. 5. Experimental results of $C_{\rm rec}(\rho_{a,s})$ and $\mathcal{N}_{\rm rec}(\rho_{a,s}(t_2))$. We scanned θ_2 while the damping parameter was fixed to $\theta_1(\eta_1 = 1) = \pi/4$ and $\theta_1(\eta_1 = 1/2) = \pi/8$ in the dashed and solid curves, respectively. Error bars come from the standard deviation over ten measurements.

polarized path is longer than the horizontally polarized one by more than the photon's coherence length, and its time delay is not balanced with respect to the lower branch. Then, vertically polarized photons cannot interfere with the lower branch when MZI closes but only the horizontally polarized photons. This mechanism prevents any coherent contribution to the coincidence detections between the vertically polarized photons of the upper branch and the ancillary ones.

In Fig. 5, upper panel, we show our experimental results for $C_{\rm rec}$ in two damping regimes. These correspond to fixing θ_1 first at $\pi/4$ (solid curve) and then at $\pi/8$ (dashed curve). The solid curve for $C_{\rm rec}$ starts at zero, which is the end value of the Markovian regime, and then it goes up to 1, thereby recovering the starting value of the Markovian process. Hence, the solid curve in Fig. 5, upper panel, can be seen as a continuation of Fig. 4. By adding further Markovian and non-Markovian steps, we would witness a periodical process. It is worthwhile to notice that there is another periodical process that we can obtain by using just the Sagnac part of our setup. Indeed, if we increase θ_1 beyond $\pi/4$ in $C_{\rm rec}(\theta_1)$ of

Fig. 4, we get the exact solid curve of Fig. 5, upper panel. This corresponds to a case in which the s qubit and the e qubit periodically exchange one excitation. In such a case, the e qubit is no longer modeling a reservoir but some two-state system. A possible physical scenario, which is modeled by this setup, could be, for instance, an ideal cavity containing a two-level atom and a single-mode photon. η_1 would then correspond to a time parametrization of the type $\eta_1 = \sin^2(\omega t)$ instead of a parametrization of the type $\eta_1 = 1 - e^{-\gamma t}$, which corresponds to an environment having infinite modes, among which one excitation ($|1\rangle_e$) is distributed [27]. Of course, it is an inherent feature of our setup that it leads to periodic processes, because we produce them with rotatory elements, the wave plates. It is by parametrizing the quantum channels in terms of transition probabilities, $\eta_{i=1,2}$, that we can address decay processes as well as oscillatory exchanges of excitations. Even though the parameters η_i are inherently periodic in our setup, i.e., $\eta_i = \sin^2(2\theta_i)$, we can model the two types of processes by properly delimiting the range in which those parameters should vary [27].

In Fig. 5, lower panel, we finally show the associated values of $\mathcal{N}_{\text{rec}}$ for the non-Markovian regimes we have explored. As we can see, the higher the damping θ_1, the higher the accessible degree of non-Markovianity.

Despite the usual experimental imperfections, our results were in good agreement with theoretical predictions. This was mainly due to the purity we could achieve for the initial states, as well as to the overall low error sensitivity of our protocol. As already pointed out, purity of the initial states was better than 92% in each experimental run. Another figure of merit, even though under the previously mentioned provisos [22], is fidelity. We obtained $F = |\langle\psi_{\text{exp}}|\psi(t_0)\rangle_{(a,s)}|^2 = 0.955 \pm 0.001$.

IV. CONCLUSIONS

In this work, we have shown the feasibility of an all-optical setup that simulates open quantum system dynamics containing Markovian and non-Markovian regimes. We implemented an ancilla-system compound state that allowed us to diagnose non-Markovianity in a relatively simple way. Indeed, by starting with a maximally entangled ancilla-system state, it is possible to employ an easily calculable quantifier of non-Markovianity to which one has direct experimental access. This quantifier is based on the relative entropy of coherence. Besides its usefulness in quantum information science, this measure appears to be a versatile tool for the study of open quantum systems.

Our approach provides additional tools for the study of non-Markovian processes and complements other studies. Indeed, the AD channel has been recently employed to study non-Markovianity in an experiment that simulates a single-photon setting by using an intense laser beam [28]. The simulated AD channel corresponded in this case to the damped Jaynes-Cummings model, which in the non-Markovian regime exhibits coherence revivals. This is in accordance with our findings, if we extend the range covered by the damping parameter η_2. Another experiment related to ours was reported in Ref. [29]. In this case, the AD process affects a two-level system that is in contact with a reservoir modeled with harmonic oscillators. Non-Markovianity is diagnosed in terms of entanglement of formation (EOF), and the corresponding dynamics is experimentally simulated by mapping the time evolution to the orientation of a HWP in an interferometric arrangement. In this case, a nonmonotonic behavior of the EOF shows up in the non-Markovian regime.

In contrast with the above cases, our implementation of the system-environment interaction contains a genuine stochastic feature. This feature comes into play through the coupling between photon polarization and spatial degrees of freedom, by which some system photons—those vertically polarized—are stochastically excluded from optical interference and so from contributing to the coherence revival of the final state with respect to the input one. This polarization-dependent action of the environment on the system somewhat resembles the implementation of system-environment interactions in purely dephasing processes. In these implementations, the photon polarization represented the system, while the environment's role was played by the photon frequency distribution. By making the latter depend on the polarization state, it was possible to generate non-Markovian regimes.

Our results show that we can achieve full coherence recovery under suitable conditions. This hints at the possibility of information protection or recovery when dealing with open quantum systems. It is an as yet unanswered question how to translate protocols such as those reported in this work into protocols that are well suited for dealing with information-carrying quantities. In any case, the concrete realization of Markovian and non-Markovian regimes helps to broaden our understanding of the dynamics of open quantum systems.

ACKNOWLEDGMENTS

This work was partially supported by the U.S. Office of Naval Research Global (ONR, Award No. N62909-19-1-2148, Grant No. GRANT12853637) . One of us (Y.Y.) gratefully acknowledges financial support from CONCYTEC-FONDECYT (Grant No. 236-2015).

[1] H.-P. Breuer and F. Petruccione, *The Theory of Open Quantum Systems* (Oxford University Press, Oxford, UK, 2007).

[2] Á. Rivas, S. F. Huelga, and M. B. Plenio, Rep. Prog. Phys. **77**, 094001 (2014).

[3] H.-P. Breuer, E.-M. Laine, J. Piilo, and B. Vacchini, Rev. Mod. Phys. **88**, 021002 (2016).

[4] T. Baumgratz, M. Cramer, and M. B. Plenio, Phys. Rev. Lett. **113**, 140401 (2014).

[5] Z. He, H.-S. Zeng, Y. Li, Q. Wang, and C. Yao, Phys. Rev. A **96**, 022106 (2017).
[6] M. A. Nielsen and I. L. Chuang, *Quantum Computation and Quantum Information*, 10th ed. (Cambridge University Press, New York, 2011).
[7] A. Streltsov, U. Singh, H. S. Dhar, M. N. Bera, and G. Adesso, Phys. Rev. Lett. **115**, 020403 (2015).
[8] J. Sun, Y.-N. Sun, C.-F. Li, G.-C. Guo, K. Luoma, and J. Piilo, Sci. Bull. **61**, 1031 (2016).
[9] B.-H. Liu, D.-Y. Cao, Y.-F. Huang, C.-F. Li, G.-C. Guo, E.-M. Laine, H.-P. Breuer, and J. Piilo, Sci. Rep. **3**, 1781 (2013).
[10] B.-H. Liu, L. Li, Y.-F. Huang, C.-F. Li, G.-C. Guo, E.-M. Laine, H.-P. Breuer, and J. Piilo, Nat. Phys. **7**, 931 (2011).
[11] J.-S. Tang, C.-F. Li, Y.-L. Li, X.-B. Zou, G.-C. Guo, H.-P. Breuer, E.-M. Laine, and J. Piilo, Europhys. Lett. **97**, 10002 (2012).
[12] S. Cialdi, D. Brivio, E. Tesio, and M. G. A. Paris, Phys. Rev. A **83**, 042308 (2011).
[13] H. Zhu, Y. S. Teo, and B. G. Englert, Phys. Rev. A **82**, 042308 (2010).
[14] S. Cialdi, M. A. C. Rossi, C. Benedetti, B. Vacchini, D. Tamascelli, S. Olivares, and M. G. A. Paris, Appl. Phys. Lett. **110**, 081107 (2017).
[15] E.-M. Laine, H.-P. Breuer, J. Piilo, C.-F. Li, and G.-C. Guo, Phys. Rev. Lett. **108**, 210402 (2012).
[16] T. Chanda and S. Bhattacharya, Ann. Phys. **366**, 1 (2016).
[17] Á. Cuevas, A. Geraldi, C. Liorni, L. D. Bonavena, A. De Pasquale, F. Sciarrino, V. Giovannetti, and P. Mataloni, Sci. Rep. **9**, 3205 (2019).
[18] N. K. Bernardes, Á. Cuevas, A. Orieux, C. H. Monken, P. Mataloni, F. Sciarrino, and M. F. Santos, Sci. Rep. **5**, 17520 (2015).
[19] C. Benedetti, A. P. Shurupov, M. G. A. Paris, G. Brida, and M. Genovese, Phys. Rev. A **87**, 052136 (2013).
[20] M. Bina, A. Mandarino, S. Olivares, and M. G. A. Paris, Phys. Rev. A **89**, 012305 (2014).
[21] A. Uhlmann, Rep. Math. Phys. **9**, 273 (1976).
[22] S. Cialdi, A. Smirne, M. G. A. Paris, S. Olivares, and B. Vacchini, Phys. Rev. A **90**, 050301(R) (2014).
[23] A. K. Rajagopal, A. R. Usha Devi, and R. W. Rendell, Phys. Rev. A **82**, 042107 (2010).
[24] Y.-N. Guo, Q.-L. Tian, K. Zeng, and Z.-D. Li, Quantum Info. Proc. **16**, 310 (2017).
[25] S. C. Hou, S. L. Liang, and X. X. Yi, Phys. Rev. A **91**, 012109 (2015).
[26] D. F. V. James, P. G. Kwiat, W. J. Munro, and A. G. White, Phys. Rev. A **64**, 052312 (2001).
[27] A. Salles, F. de Melo, M. P. Almeida, M. Hor-Meyll, S. P. Walborn, P. H. Souto Ribeiro, and L. Davidovich, Phys. Rev. A **78**, 022322 (2008).
[28] M. H. M. Passos, P. C. Obando, W. F. Balthazar, F. M. Paula, J. A. O. Huguenin, and M. S. Sarandy, Opt. Lett. **44**, 2478 (2019).
[29] F. F. Fanchini, G. Karpat, B. Cakmak, L. K. Castelano, G. H. Aguilar, O. J. Farias, S. P. Walborn, P. H. Souto Ribeiro, and M. C. deOliveira, Phys. Rev. Lett. **112**, 210402 (2014).